We are IntechOpen, the world's leading publisher of Open Access books Built by scientists, for scientists

6,900
Open access books available

185,000
International authors and editors

200M
Downloads

Our authors are among the

154
Countries delivered to

TOP 1%
most cited scientists

12.2%
Contributors from top 500 universities



WEB OF SCIENCE™

Selection of our books indexed in the Book Citation Index in Web of Science™ Core Collection (BKCI)

Interested in publishing with us?
Contact book.department@intechopen.com

Numbers displayed above are based on latest data collected.
For more information visit www.intechopen.com



Chapter 3

Thin-Film Magneto-Impedance Sensors

Alfredo García-Arribas, Eduardo Fernández and David de Cos

Additional information is available at the end of the chapter

http://dx.doi.org/10.5772/intechopen.70084

Abstract

We review the state-of-the-art of thin films displaying the magneto-impedance (MI) effect, with focus on the aspects that are relevant to the successful design and operation of thin film-based magnetic sensors. After a brief introduction of the MI effect, the materials and geometries that maximize the performance, together with the measurement procedure for their characterization, are exposed. A nonexhaustive survey of applications is included, mostly with the aim of displaying the capabilities of thin film structures in the field of magnetic sensing, and the variety of topics covered by them. A special emphasis is made on some concepts that are not commonly treated in the literature, such as the influence of the measuring circuit on the magneto-impedance ratio, the geometry optimization by means of numerical simulation by finite element methods, or noise measurements on thin films. Additionally, a brief description of the patterning procedure by photolithography is included, since the major advantage of thin film sensors over other types of magneto-impedance materials as ribbons or wires is the possibility of patterning the sensible element in micrometric shapes, and most of all, their easy integration with the interface microelectronic circuitry.

Keywords: magneto-impedance, thin film, magnetic sensor, photolithography, finite element methods

1. Introduction

The giant magneto-impedance (MI) effect accounts for the large change of the electrical impedance experienced by a soft magnetic material when subjected to an external magnetic field. It was proposed as a very sensitive method to detect small magnetic fields during the 1990s [1, 2]. However, the basic underlying principle is a completely classical electromagnetic effect that was already studied by Lord Rayleigh in 1887 [3] and with much greater detail by Kittel in 1946 [4]. It is based on the so-called skin effect, which accounts for the limited

INTECH
open science | open minds

© 2017 The Author(s). Licensee InTech. This chapter is distributed under the terms of the Creative Commons Attribution License (http://creativecommons.org/licenses/by/3.0), which permits unrestricted use, distribution, and reproduction in any medium, provided the original work is properly cited. CC BY

penetration on conductive materials of the electromagnetic field associated with an alternating current flowing through them. The exponential decrease of the amplitude of the fields from the surface of the conductor is characterized by the penetration depth δ given by

$$\delta = 1/\sqrt{\pi f \sigma \mu}, \tag{1}$$

where f is the frequency of the alternating current and σ and μ are the conductivity and the magnetic permeability of the material, respectively. The effective cross-section of the sample for the flow of the alternating current depends on the magnitude of the penetration depth. Therefore, the skin effect determines the impedance of the specimen, and if the sample is magnetic, the external magnetic field modifies the permeability and produces the magneto-impedance effect. In summary, the basics of MI are described by Maxwell equations and explained in classical treatises on electromagnetism [5, 6].

If the geometry of the sample is simple enough, the Maxwell equations can be solved analytically to obtain the impedance. In the case of a homogenous sheet of thickness 2a and infinite width and length, the result is [7]

$$Z = R_{dc} \sqrt{j\theta} \coth \sqrt{j\theta} \tag{2}$$

being R_{dc} the dc resistance, $j = \sqrt{-1}$ (the imaginary unit), and $\theta = a\sqrt{2\pi f \sigma \mu} = \sqrt{2}\, a/\delta$. A similar expression involving Bessel equations can be obtained for wires [7].

It is to be noted that the permeability involved in expressions (1) and (2) is the one responding to the alternating magnetic field created by the flowing current (**Figure 1**), which is transversal to the direction of current flow and is usually denominated transverse permeability.

The magneto-impedance is typically quantified as a difference ratio with respect to a reference impedance value as

$$\text{MI}\,(\%) = \frac{Z - Z_{low}}{Z_{low}} \times 100 \tag{3}$$

where Z_{low} is almost always taken as the lowest measured value of the impedance. Habitually, Z_{low} corresponds to the impedance of the sample when it is magnetically saturated and its relative permeability is close to 1: $Z_{low} = Z_{sat} = Z(\mu_0)$. Experimentally, Z_{low} usually corresponds to the impedance measured at the maximum applied magnetic field $Z_{low} = Z\,(H_{max})$, which is supposed to magnetically saturate the sample. It can also be taken as the impedance at zero field $Z_{low} = Z(H = 0)$, if the MI curve is double-peaked (**Figure 1**).

One of the figures of merit for MI is the maximum value of the magneto-impedance given by Eq. (3) MI_{max}, which is reached when the value of Z is maximum. For a given frequency, and according to Eq. (1), this occurs when the permeability is maximum and the penetration depth is minimum. Therefore, the magnetization processes of the sample, which determine the magnitude of the transverse permeability, are paramount in achieving large MI_{max} ratios.

The second figure of merit is the maximum sensitivity s_{max}, which is actually the most important for applications. It expresses the maximum change of impedance experienced by the

http://dx.doi.org/10.5772/intechopen.70084

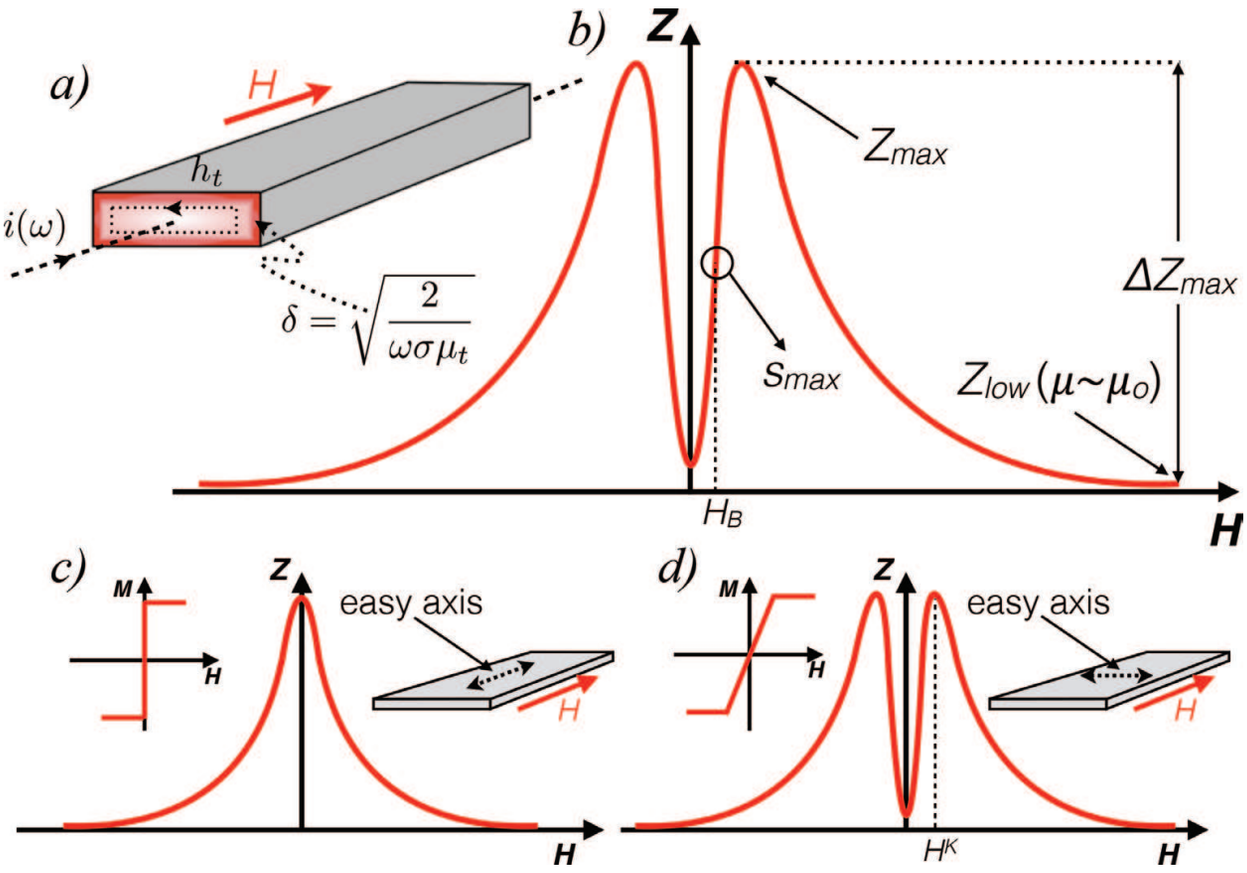


Figure 1. (a) Scheme of the magneto-impedance effect in a planar sample: the alternating current i accumulates on the surface due to the skin effect, whereas its magnetic field h_t excites the material according to its transverse permeability μ_t, which is modulated by the externally applied magnetic field H. (b) Typical magneto-impedance curve: the maximum impedance occurs when μ_t is largest, and the minimum when it is magnetically saturated. The maximum sensitivity s_{max} takes place at the point of the largest slope of the $Z(H)$ curve. The sample must be biased with a field H_B to obtain the maximum field sensitivity. (c) Single-peaked MI curve when the magnetic field H is applied in the direction of the magnetic easy axis (longitudinal anisotropy). (d) Double-peaked MI curve in the case of transverse anisotropy.

sample when the magnetic field acting on it varies, that is, the maximum slope of the $Z(H)$ curve. It also depends on the magnetization process. The most usual cases in planar samples are schematized in **Figure 1(c)** and **(d)**. In a sample with longitudinal anisotropy, the magnetization easy axis lays in the direction of the applied field and the flow of current. The maximum transverse permeability occurs at $H = 0$, and the $Z(H)$ curve presents a single peak. If the sample presents transverse anisotropy, the maximum transverse permeability takes place at the anisotropy field H^k, defined as [8]

$$H^k = \frac{2K}{\mu_0 M_s}, \tag{4}$$

where K is the anisotropy constant and M_s the saturation magnetization. This is the preferred case, since the curve $Z(H)$ presents two peaks and can display a great sensitivity if MI_{max} is large and H^k is small. In thin film MI sensors, it is extremely important to obtain a well-defined transverse magnetic anisotropy.

2. Thin film MI samples

2.1. Sample geometry

The best samples for large MI effect are amorphous wires and glass-coated microwires with very small negative magnetostriction [9, 10], especially those in which the configuration of the magnetic domains favors a large circular (transverse) permeability [11]. Values up to MI_{max} = 500% are reported in the best homogenous wires. MI has been also actively studied in amorphous ribbons [12, 13]. In both cases (wires and ribbons), the MI takes large values at frequencies of tens or hundreds of kHz, when the penetration depth equals the thickness of the sample, in the order of tens of microns. MI in thin films, however, requires much larger frequencies, typically of the order of 1 GHz for films of about 1 μm thick. This situation has two important consequences that will be discussed in the following sections: first, the measuring circuits for the characterization of the MI response must be adapted for such elevated frequencies, and second, from the point of view of the properties of the thin film material, adequate strategies must be adopted to increase the thickness of the sample without deteriorating the soft magnetic behavior.

To increase the magnitude of the MI effect in thin film materials, a sandwiched structure with a nonmagnetic conductor between two magnetic layers was early proposed [14–16], in which the magneto-inductive effect, created by the large permeability of the magnetic layers, allows to override the pure skin effect and achieve large impedance variations at moderate frequencies. The advantages of this layered structure were also incorporated in wire-shaped specimens to achieve MI ratios of 800%, the largest reported in the literature [17]. Analytical expressions similar to Eq. (2), but more complicated, can be obtained for some sandwiched geometries by imposing the suitable boundary conditions at the interface of the materials [18]. In sandwiched structures it is possible to devise two main configurations as schematized in **Figure 2**. If the outer magnetic layers completely enclose the central conductor, the layout resembles that of a core-shield wire, in which the magnetic flux created by the current encounters a closed path with high permeability. In contrast, the open-flux configuration, in which the magnetic and central layers have the same width, makes the flux created by the current

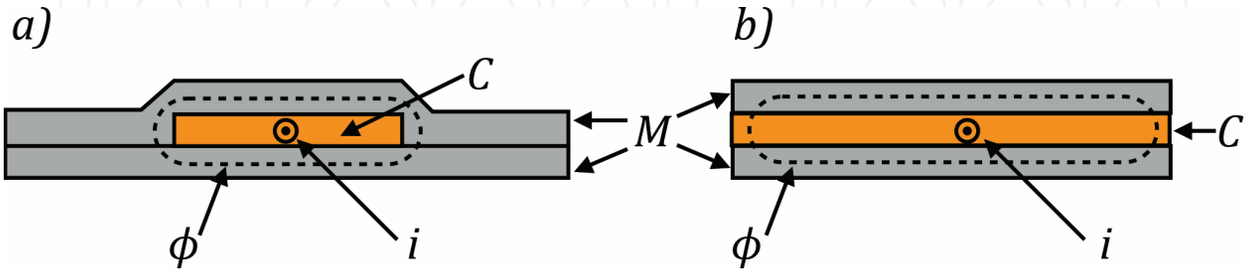


Figure 2. The sandwich structure *M*/*C*/*M* (*M* = magnetic layer, *C* = conductive, nonmagnetic layer) enhances the magneto-inductive response of thin film samples, overriding the poor influence of the skin effect at moderate frequencies (in the range of MHz). The figure shows the cross-section of two possible configurations for sandwiched structures. In (a) the magnetic layers enclose the central conductor, providing a high permeability closed path for the magnetic flux φ generated by the alternating current *i* (flowing perpendicular to the page). In (b), the flux lines must close by a nonmagnetic medium, reducing the magneto-inductive effect, but this structure is much easier to fabricate.

cross a low permeability path. The flux leakage worsens the MI behavior [19], but the open-flux configuration can be fabricated in a single step, which makes it preferable over the closed-flux one. Besides, the direct comparison between both configurations demonstrates that the MI performance gain found in closed-flux is not significant due to additional problems arising from the increased thickness of the magnetic layers in the edges of the structure [20].

Thin film MI materials are commonly patterned to adjust their lateral dimensions to the desired shape. The usual geometry is in the form of rectangular stripes, but other shapes as meanders or ellipsoids are used depending on the application. The patterning can be performed during the deposition or using photolithography techniques. More details will be given in Section 2.3.

2.2. Thin film MI materials

The most successful MI materials, in the form of wires and ribbons, are made from amorphous alloys (Fe-Co-Si-B or similar), rapid quenched from the melt. These materials, obtained by other methods, have also been used for thin film MI structures. In fact, values of MI_{max} close to 700% were early reported from a closed-flux sandwiched structure of CoSiB layers [21]. Such extraordinary performance was obtained due to the large thickness of the magnetic layers (2 μm) and the use of isolation SiO_2 layers between the central conductor and the outer magnetic layers. Also, amorphous FeSiB [22], CoNbZr [23], and FeCuNbSiB [24] films have been investigated in MI structures. But the dominant tendency in MI thin film structures is to use Permalloy (Py) as magnetic layer. With a nominal composition of $Fe_{20}Ni_{80}$, Permalloy is a very soft magnetic alloy with large permeability, no crystalline anisotropy, and nearly vanishing magnetostriction, which are key properties for great MI performance. Besides, the constituents of Py are abundant and cheap and its use in MI devices benefits from the intense research performed toward enhancing anisotropic magnetoresistance (AMR) sensors that use Py as base material [25].

Permalloy in the form of thin film is obtained mainly by vapor deposition methods. The films with a small thickness are satisfactorily soft, but the growth of thicker films is affected by the development of a columnar structure that defines an easy magnetization axis in the direction perpendicular to the plane of the sample. In this situation, the sample enters what is called a transcritical state [26], observed also in amorphous films [27], which ruins the magnetic softness and results severely detrimental for MI performance, since MI requires both magnetic softness and increased sample thickness. Therefore, it is very important to determine the optimum preparation conditions, as well as the limiting Py single-layer thickness that can be reached before entering the transcritical state. In low pressure sputtering deposition, this thickness is determined to be about 170 nm [28]. To increase the total effective thickness, it has been proposed to use thin spacers between successive Py layers, creating a thick magnetic multilayer in which all the Py films are below the critical thickness [29, 30]. Different materials are used as spacers (Ti, Cu, Ag, etc.). Their nature and optimum thickness has been investigated [31] and the usefulness of this approach proven [32]. **Figure 3** displays the typical layer configuration of a high performance MI structure, which combines the sandwich layout to take advantage for the magneto-inductive effect, with outer magnetic parts composed of a multilayer Py/Ti structure in which the Py layers are below the critical thickness.

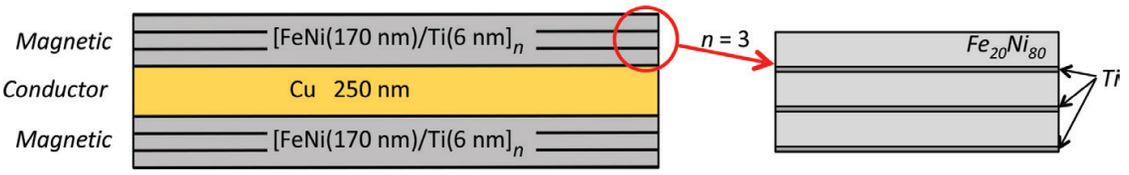


Figure 3. Scheme of the cross-section of a multilayered sandwiched structure with open-flux configuration: the outer magnetic layers are composed of Permalloy ($Fe_{20}Ni_{80}$) films below the transcritical thickness separated by thin titanium spacers. The central conductive layer is nonmagnetic.

Besides the sensitive element, other materials can play a role in MI devices. The obvious ones are metals for electric contacts. More exceptional are materials devised to produce a biasing effect on the MI element. As observed in **Figure 1**, the largest sensitivity obtained with a small bias field H_B is applied to the sample. In laboratory experiments, it is provided by an external coil; but for a functional device, biasing by an integrated thin film permanent magnet [33] or by the polarizing effect of the exchange bias effect has been demonstrated [34–36].

2.3. Fabrication of MI structures

Thin film MI structures are most commonly fabricated by physical vapor deposition methods, although electrodeposition [37] or flame plating [38] has also been used. Sputtering is preferred over evaporation. The process parameters (RF or DC sputtering, Ar pressure, power, deposition time, etc.) depend on the equipment used and the nature of the desired material. Glass or silicon wafers are used as substrates, although polymers are increasingly being used with the onset of flexible electronics [39–42]. As large sensitivity relies on a well-defined transverse anisotropy, an in-plane magnetic field is usually applied during deposition. The deposition process creates a continuous film on the substrate. For measurements and applications, the substrate can be cut into the desired shape, usually rectangular. Alternatively, metallic masks with perforated motives (rectangular slits, for example) can be used over the substrate during the deposition. However, thin film technology is excellently adapted to the patterning procedures of the microelectronic industry. Photolithography allows creating arbitrary shapes with extraordinary lateral resolution and very well-defined borders. Basically, photolithography transfers the desired pattern defined as opaque or transparent motives on a mask into a photosensitive resist deposited on the substrate. The resist is exposed to ultraviolet (UV) light (365 nm from Hg lamps in laboratory systems) through the mask and is sensitized in the illuminated regions, changing its resistance to a given chemical (developer). Therefore, upon developing, the nonresistant parts of the resist are removed, leaving the desired pattern on the substrate. The patterned resist can be used to shape the thin film in two different ways [43], exemplified in **Figure 4**. In *etching* processes, the material is deposited as a continuous film on the substrate and the resist is patterned on top of it afterwards. The material not protected by the resist is removed using a chemical or plasma etching. In a *lift-off* process, the resist is patterned directly on the substrate and the material is deposited afterwards on top of it. When the resist is dissolved (in acetone or similar), the material deposited on top of it is peeled off, leaving the desired pattern on the substrate. Lift-off requires an inwards profile in the patterned resist in order to produce well-defined, sharp edges, as illustrated in **Figure 4(b)**.

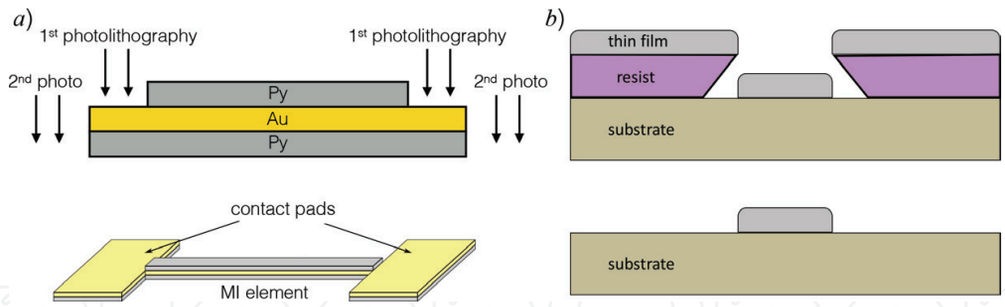


Figure 4. Example of photolithography processes to pattern thin film MI elements. (a) Photolithography is used to define the areas of the continuous film to be etched. The figure schematizes the two-step process to create the displayed structure. The first lithography defines the form of the element. The second reveals the central Au layer in the contact regions. Etching is performed by ion-milling in this case. (b) Illustration of the lift-off process in which the photoresist is patterned prior to the deposition of the thin film material. The inward profile of the resists facilitates the creation of sharp borders in the patterned material when the resist is dissolved, eliminating the material deposited on top of it.

Photolithography can be used to pattern MI samples in any desired shape. Although rectangles are most usual, meanders [37, 44] or ellipsoids [45] are also reported. Several photolithography steps can be performed sequentially to add pads for electric contacts, produce more complicated systems as closed-flux structures, or to integrate the sample in a functional device with the conditioning electronics. For example, successive photolithography steps are done to integrate a MI sample into a coplanar transmission line [45, 46].

The search for the optimum configuration of MI structures implies evaluating the impact on the MI performance of many fabrication parameters. For instance, in Py-based sandwiched structures, the effect of open- or closed-flux configuration [20], the thickness of the magnetic layers [47], the nature of the spacers between the magnetic layers [31], and the different thickness of the central conductor [48] have been experimentally assessed. The lateral dimensions of the samples play a fundamental role in the performance as well. While maximum miniaturization is beneficial for the development of MI-based microsensors, downsizing has large influence on the magnetic properties and general MI performance. For instance, the shape anisotropy in elongated samples competes with the transverse anisotropy induced during the preparation, modulating the sensitivity of the sample [49], and producing an inhomogeneous behavior over the sample that can be compensated by shaping the sample in the form of ellipsoids [45] or limiting the usable region of the device [50]. Reducing the lateral size increases the flux leakage in open-flux sandwiched structures [51]. Besides, the reduced size modifies the magnetic domain structure, since the influence of closure domains becomes increasingly important as the width of the sample is reduced [52]. At the present moment, the MI performance diminishes considerably in identical samples upon size reduction [53].

3. MI measurements in thin films

3.1. Measuring impedance at high frequency

Sandwiched thin films materials display large MI variations in the frequency range of tens to hundreds of megahertz (MHz). Operating in this regime demands using high-frequency

techniques, which involve adapting both the experimental set-ups and the mathematical treatment of the acquired data [54]. With low frequency signals the voltage and current present the same value in every point of the circuit at any given moment. However, at high frequencies, if the measuring circuit length is comparable to the wavelength λ of the electromagnetic signal ($\lambda = v/f$, v being the velocity of the light in the transmission medium and f the frequency of the signal), the electric parameters can be different in different parts of the circuit at the same time, and the measured impedance can oscillate between minimum and maximum values depending on the operating frequency. These results are determined mainly by the propagative effects of the signal along the transmission lines, and only very weakly by the actual impedance of the sample under test. Determining the impedance at high frequency requires using specific equipment, such as network analyzers or specialized impedance-measuring systems. The measuring circuit, including the sample holder, should be made of transmission lines (usually, coaxial cables or wave guides). The transmission lines adapted to planar samples are the microstrip and the coplanar lines displayed in **Figure 5**. The microstrip line consists of a narrow strip of flat conductor on a dielectric substrate with the ground conductor in the opposite face. In the coplanar transmission line, the main conductor and the ground are in the top face. In the case of the coplanar line shown in **Figure 5(b)**, both the sample and

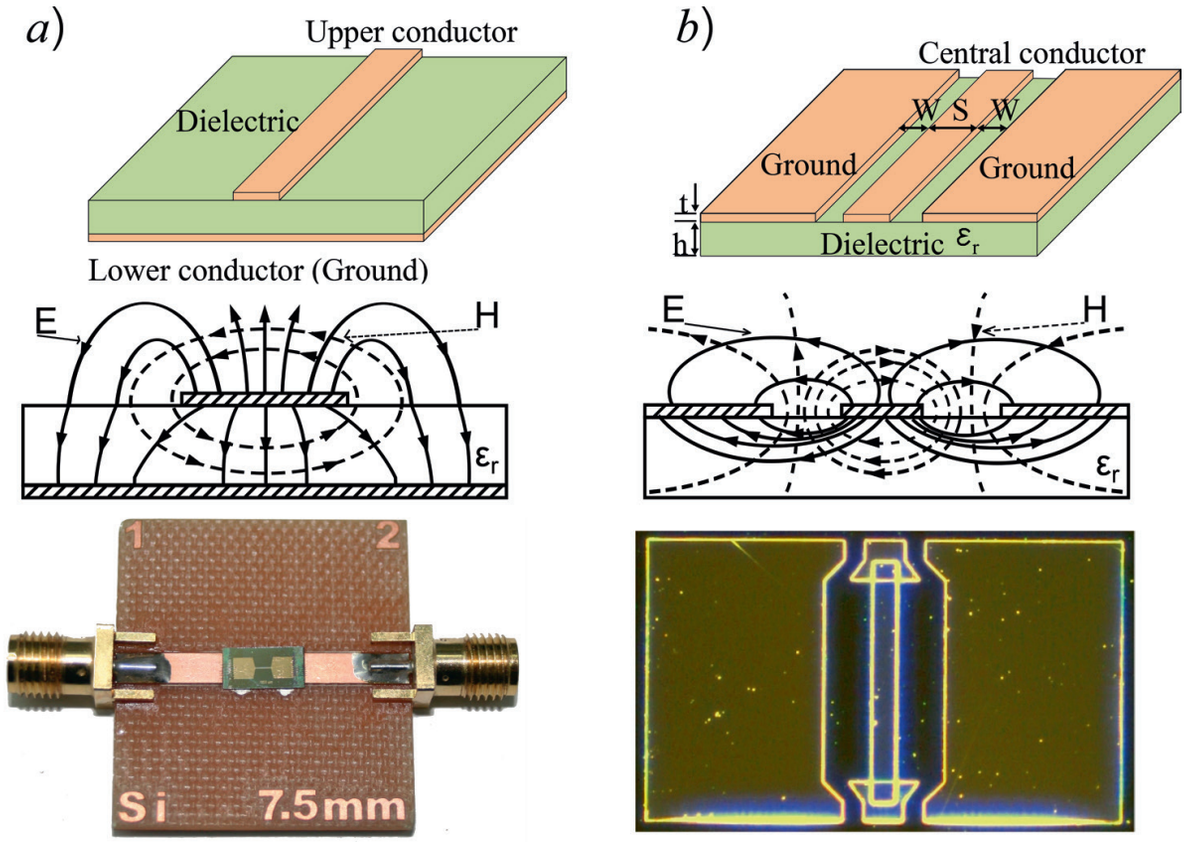


Figure 5. Transmission line-based MI measurement test fixtures. (a) Microstrip line composed by the top conductor and the bottom ground plane, supporting quasi-TEM (transverse electromagnetic mode) waves. The sample is inserted between two portions of line. (b) Coplanar transmission line, with the main conductor and the ground on the topside. In this case, the sample and the conductors of the coplanar line are fabricated by photolithography at the same time.

the line are fabricated by photolithography and the measurements are performed on wafer in a probe station [46]. **Figure 5(a)** displays a usual MI measuring test fixture in which the MI sample is inserted between two sections of a microstrip line, with SMA connectors on both sides to which coaxial cables are attached to connect to the network analyzer.

When measuring with the test fixture displayed in **Figure 5(a)**, standard calibration procedures are employed to eliminate the contribution of the coaxial cables. However, at the measuring frequencies, additional corrections should be applied to eliminate the propagation effects brought about by the portions of the line of the text fixture. The complete details are given in Ref. [54], but **Figure 6** exemplifies how the measured impedance as a function of the frequency is affected by propagation effects and how they can be corrected.

3.2. Impedance as a function of the frequency and the impact of the measuring circuit on MI

MI curves are measured as a function of the magnetic field, which is produced typically by a pair of Helmholtz coils. Using a network (or impedance) analyzer, the real and imaginary parts of the impedance can be measured as a function of the frequency, which can give us a useful insight about the MI effect in thin films. **Figure 7** shows the impedance as a function of the frequency corresponding to a Py/Au/Py sample with transverse anisotropy, measured in a microstrip line (the samples correspond to those of Ref. [55]). The real and imaginary parts of the impedance are plotted at two selected values of the applied magnetic field, $H = 0$, at which the transverse permeability is μ_0, and $H = H^k$, at which the permeability is maximum. First,

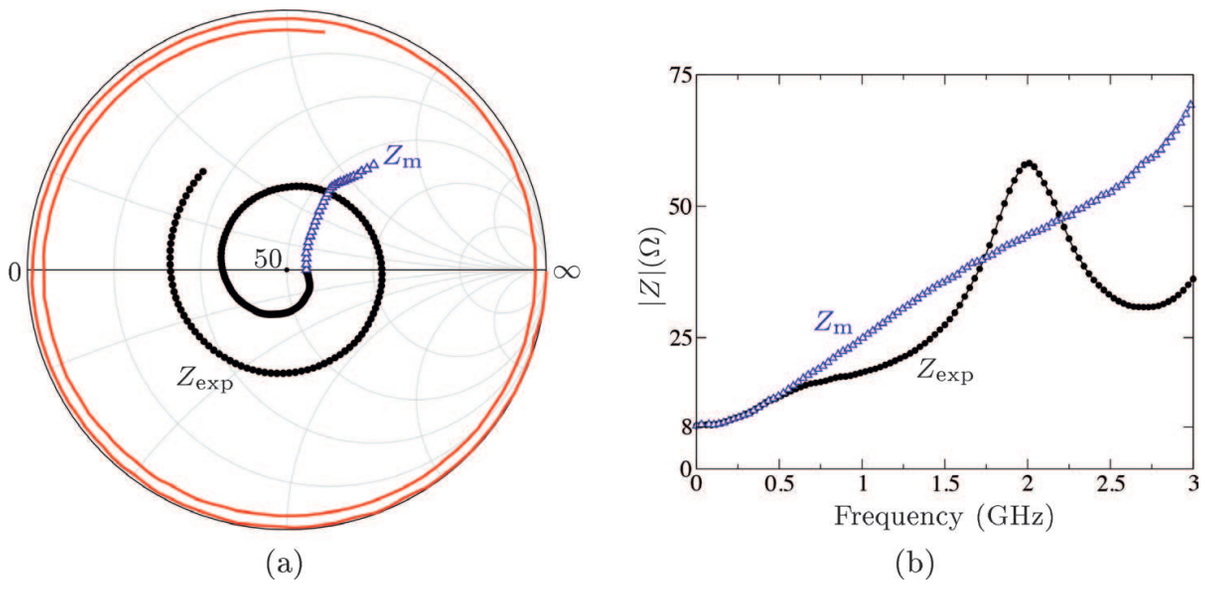


Figure 6. Effect of propagation on impedance measurements and correction. (a) The direct measurement of the impedance of the test fixture with the sample inserted, as a function of the frequency, is plotted on a Smith chart (black circles). Much of the spiral behavior is caused by the portion of the transmission line as observed in the red solid curve, measured with the sample removed from the test fixture. With the suitable correction [54], the impedance of the sample as a function of the frequency can be calculated (blue triangles). (b) The impedance directly measured Z_{exp} (black circles), without corrections, is represented as a function of frequency, showing resonance peaks caused by propagative effects. The corrected impedance Z_m (blue triangles) presents a monotonous behavior.

we show that, although the magneto-inductive effect dominates in sandwiched structures, the skin effect is also important. **Figure 7(a)** shows that the real part at $H = 0$ is constant as a function of the frequency, corresponding to the resistance of the sample (with μ_0, the penetration depth is much large than the thickness of the magnetic layer). In contrast, for $H = H^k$, the real part increases with the frequency due to the skin effect, since the penetration depth is smaller than the thickness of the magnetic layers with large permeability. The relative change of the real part of the impedance keeps growing with the frequency. Second, we observe the extraordinary importance of the external impedance in the performance of MI. The imaginary part of the impedance at $H = 0$ increases linearly from $f = 0$. The slope corresponds to the external inductance of the circuit composed by the sample and the ground plane in the microstrip line [56]. With $H = H^k$, the imaginary part increases hugely for frequencies below 100 MHz, giving a very large impedance change ratio, but afterwards it increases with the same slope as for $H = 0$, because it is dominated by the external inductance that does not depend on the magnitude of the magnetic field. Therefore, the relative change of the imaginary part decreases with frequency. In absolute value, the MI would increase with frequency following the trend

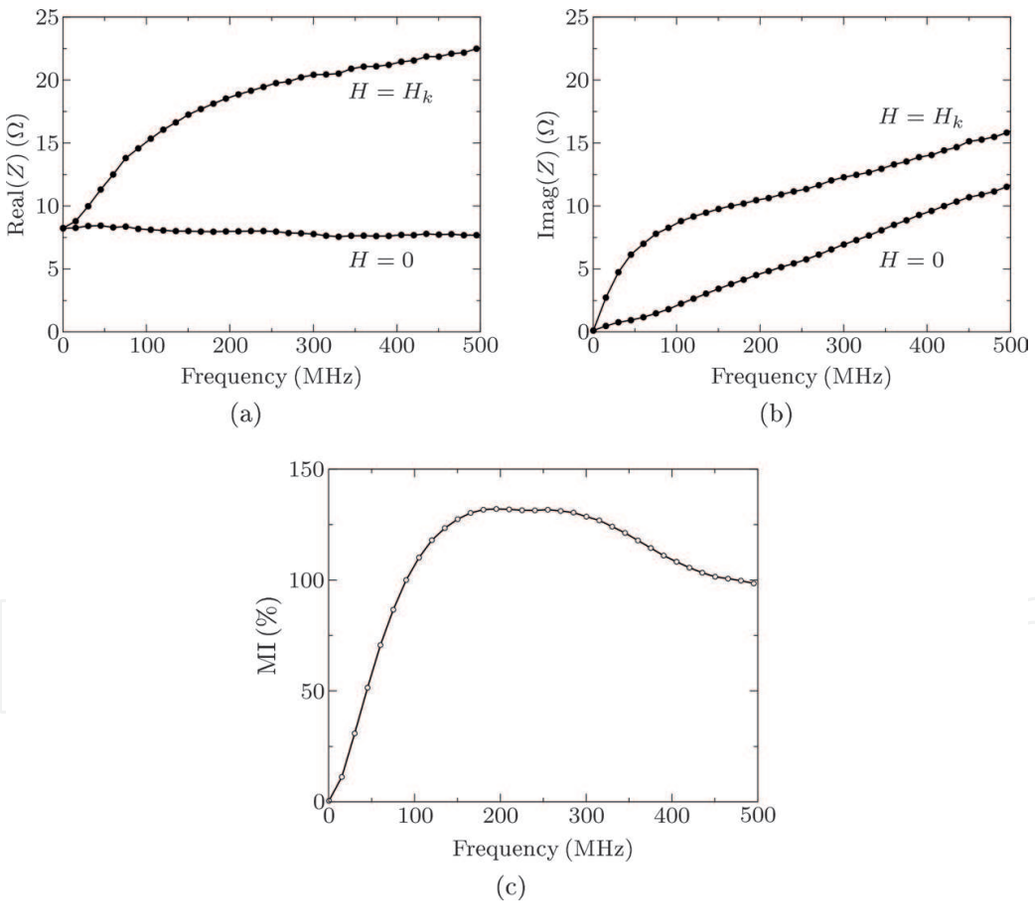


Figure 7. Selected results of the measured impedance as a function of the frequency for a Py/Au/Py multilayer [55]. (a) Real part measured at $H = 0$ and $H = H^k$, where the permeability is large, showing the importance of the skin effect. (b) Imaginary part measured at $H = 0$ and $H = H^k$. The linear increase is caused by the external self-inductance of the measuring circuit. (c) Absolute value of the magneto-impedance. It shows a maximum at approximately the frequency at which the value of imaginary part (ruled by the external inductance) equals the real part: the influence of the impedance added by the measuring circuit limits the maximum MI ratio that can be measured.

of the real part, but it is limited by the decrease of the imaginary part, which is caused by the external inductance. In fact, the maximum of the MI as a function of the frequency takes place at frequencies at which the values of the imaginary and real parts become approximately equal. If the imaginary part is kept low, by reducing the external inductance, the MI can reach larger values, because it would continue growing further with increasing frequency.

It is important to clarify that there is no way of completely avoiding the detrimental effect of the external impedance: for any measurement, or for any application, the sample must be inserted in a circuit that necessarily produces the undesired contribution to the total impedance. Transmission lines are probably the minimum measuring circuit that can be used, but they also produce an important contribution (larger in microstrip than in coplanar lines) that must be taken into account for applications or when analyzing the properties of MI materials and structures. Evidently, the importance of the external contribution in experimental MI measurements explains why the extremely large values of MI predicted by the theory are never reached. As a side effect, we see that the performance rating of materials based purely on their MI ratio is probably meaningless, because the measured values depend heavily on the measuring system. It is possible to apply specialized methods to extract the intrinsic impedance of the sample (a process called de-embedding) for the microstrip [57] and the coplanar cases [46]. This produces much larger MI values and allows, in principle, to compare measured MI values with theoretical predictions.

4. Numerical simulations by finite element method

The MI behavior can be described analytically for simple geometries and, with important assumptions, by expressions similar to Eq. (1) derived from the Maxwell equations. The description can be improved by incorporating models for the magnetization process, the dynamical behavior of the magnetization, and some other effects [58–60]. The pure theoretical analysis allows gaining insight in the involved phenomena, but fails to accurately describe the experimental results. In fact, the theory predicts values for the MI ratio of the order of 10^4% [61, 62] that have never, by far, been observed. This discrepancy is caused first by nonideal conditions on real samples: complex domain structure, finite size, etc. But most importantly, the main cause for this huge difference is that the proposed theories do not reflect the actual measurement conditions. As explained in the previous section, in a real experimental set-up, the measuring circuit imposes a contribution to the measured total impedance that drastically reduces the MI_{max} ratio, even if the circuit is simplified to the minimum expression. A rather complex data reduction process can be used to extract the intrinsic MI response from the sample, eliminating the contribution of the circuit [46, 57], or alternatively, this contribution can be incorporated in the theory [36]. Numerical simulations can overcome some of these problems and offer results closer to the experiment and serve as a guide for device optimization.

Finite element methods (FEMs) are used to solve the differential equations governing many different types of problems in completely arbitrary geometries. For electromagnetic problems, given the material properties and the appropriate boundary conditions, FEM codes can

numerically calculate the electrical impedance of the simulated system. If the dependence on the applied magnetic field of the material properties (essentially the magnetic permeability) is specified, FEM can be used to determine the impedance as a function of the magnetic field $Z(H)$, and the MI ratio according to Eq. (3) [63]. However, to analyze the MI performance of different sample configurations, it is sufficient to use FEM to calculate the impedance for two extreme values of the permeability, the largest μ_{max} (that would correspond to the value of the maximum transverse permeability) and the lowest, which equals to μ_0 when the sample is saturated. This allows to calculate MI_{max} as

$$MI_{max}(\%) = \frac{Z(\mu_{max}) - Z(\mu_0)}{Z(\mu_0)} \times 100 \quad (5)$$

This approach has been used, for example, to examine the performance difference between open- and closed-flux sandwiched structures [20] and to determine the best combination of layer thickness to maximize the MI ratio [53]. The complete three-dimensional (3D) geometry of MI structures can be simulated using commercial FEM software packages as COMSOL [63, 64]. 3D modeling is interesting because it allows, in principle, to account for the effect of shape anisotropy on MI (although no published work has taken advantage of this, yet). If the simulation makes the approximation that the sample is infinite in length, the modeling can be performed in two dimensions (2D), using much less computational resources [65, 66]. The authors routinely use the free 2D software package FEMM [67] to perform FEM simulations. When the simulation cases are numerous or require heavy computing, they use the xfemm implementation of the same code [68] that can be run in a mainframe computer. This FEM program is designed to solve low-frequency electromagnetic problems, in the sense that it implements the Maxwell equations disregarding the displacement current. Therefore, it cannot account for propagation effects and, when solving magnetic problems, it does not consider the dielectric properties of the materials, but it can simulate accurately MI problems in which the skin and magneto-inductive effects are dominant. For a complete simulation of the electromagnetic problem, including propagation and dielectric properties, a *full-wave* program is necessary.

FEM simulations can reproduce quite accurately the experimentally measured MI behavior provided that the simulated problem resembles the experimental conditions. This means that the simulation must include the contribution of the measuring circuit in which the sample is inserted. One of the most popular measuring test fixtures for planar samples, including thin films, is that based on microstrip transmission lines. **Figure 8** schematizes the 2D simulation problem of a thin film structure. Note that, due to the symmetry, only half of the problem must be simulated. The simulation includes, below the sample, the ground conductor of the transmission line, which is made of pure copper, and the dielectric, although it is treated as a dummy material with permeability μ_0, in the same manner as the air filling the rest of the simulation domain. What is important in the simulation is the amount of impedance that the measuring circuit adds to the impedance of the sample. It is mainly produced by its self-inductance, which depends on the geometry of the circuit. The simulation domain must be limited to maintain the problem under reasonable computation demands. Therefore, appropriate boundary conditions

http://dx.doi.org/10.5772/intechopen.70084

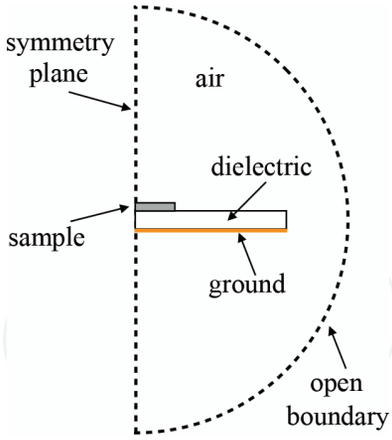


Figure 8. Sketch of the 2D FEM problem for calculating the impedance of a thin film sample (the drawing is not at a real scale). The simulation domain includes the sample and the microstrip line in which it is inserted for real MI measurements. Only half of the problem needs to be simulated thanks to the symmetry. Open boundary conditions are applied to reduce the size of the simulation domain without losing accuracy [67].

must be imposed in the limits of the domain representing the values of the fields over them. This can be problematic in our geometry because the fields are extended, in principle, to the infinite. FEMM offers different possibilities for adequate boundary conditions dealing with that situation, such as the open boundary conditions, represented in **Figure 8**. Other software packages offer similar solutions as the infinite elements used in COMSOL.

FEM calculations are based on discretizing the simulation domain in small portions (triangles in 2D). In principle, the finer the meshing, the more accurate the solution is. However, there is a compromise with computation time and the best strategy is to refine the mesh only where it is important for the solution. Commercial programs include automatic, adaptative, refinement algorithms. In FEMM, this must be done manually. For MI problems, it is especially important to choose a mesh fine enough to accurately determine the fields in the regions where the skin effect is important. As a rule of thumb, we usually chose a mesh 10 times smaller than the penetration depth given by Eq. (1) at each frequency in the appropriate regions.

To calculate the impedance in our FEMM problem, a current is flowed through the sample, perpendicular to the plane of simulation. The current returns in the opposite direction through the ground conductor. Apart from the geometry of the sample, its material properties must be specified. The relevant ones are the conductivity ($\sigma_{Py} = 4.5 \times 10^6$ S/m for Py and $\sigma_{Ti} = 2.38 \times 10^6$ S/m for Ti) and the magnetic permeability. As explained before, the impedance is calculated for two different values of the permeability, μ_{max} and μ_0, assuming the sample is isotropic. This calculation is performed for different frequencies, allowing to obtain MI_{max} versus frequency curves as the ones displayed in **Figure 9**. In this example, the agreement between measurement and simulation is exceptional, up to a frequency of 150 MHz. This degree of coincidence has been secured by performing simulations with different values of μ_{max} until the results matched. FEM simulations therefore constitute a method to determine the maximum value of the transverse permeability of the sample, which is close to $\mu_{max} = 4300\ \mu_0$ in this case. For higher frequencies, there is an increasing discrepancy between simulated and measured values, which can be attributed to the frequency dependence of the permeability.

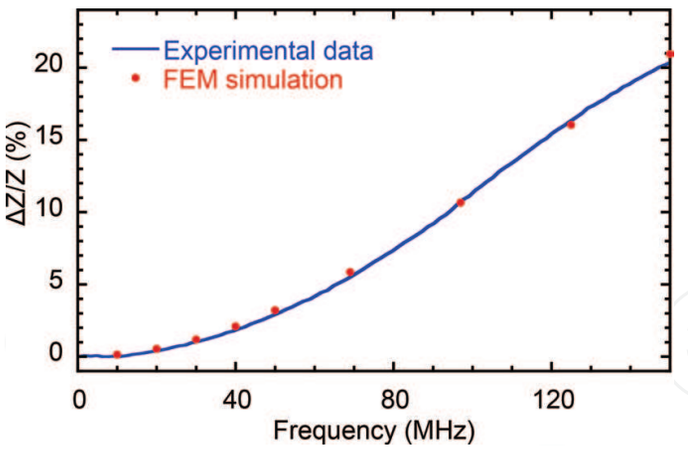


Figure 9. Impedance ratio as a function of the frequency for a thin film multilayer sample [Py (100 nm)/Ti (6 nm)]$_3$/Py (100 nm)]. The agreement between the experimental data and the FEM-simulated values allows determining the value of the transverse permeability of the Py layers.

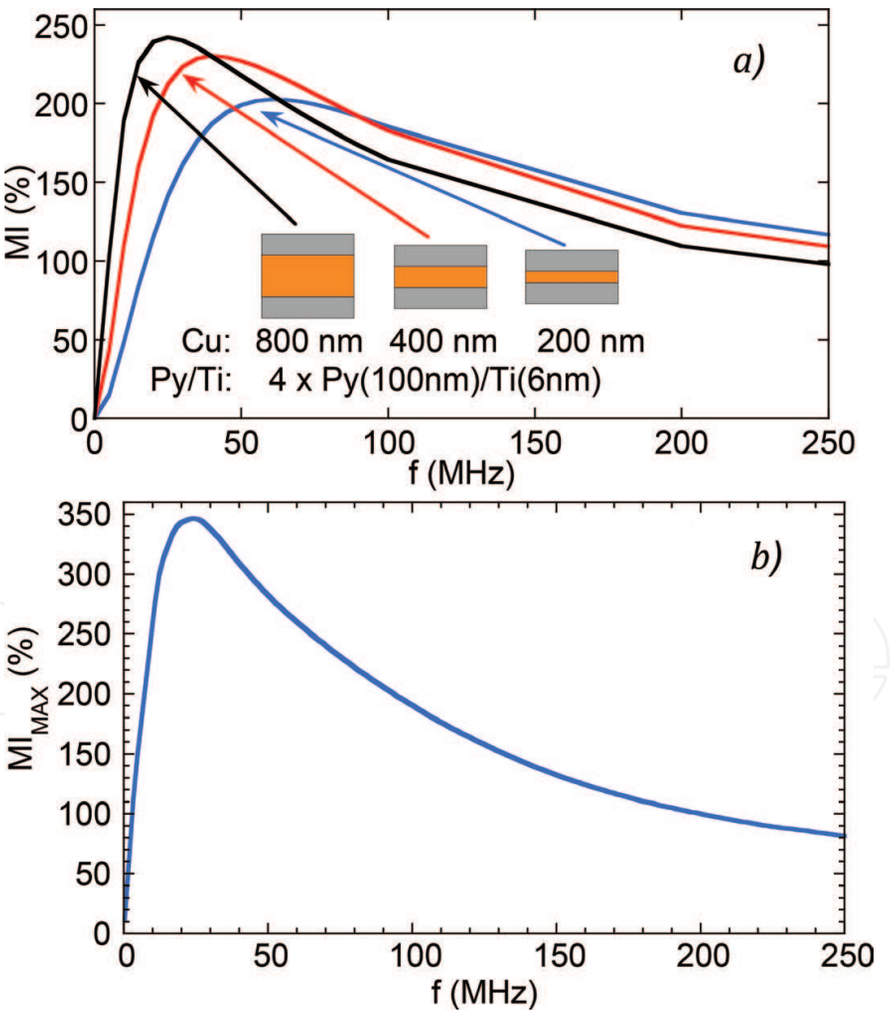


Figure 10. (a) FEM results for sandwiched samples with different thicknesses of the central conductor. The simulations were performed to determine the geometry for maximizing the MI ratio [53]. (b) MI ratio measured in a sample 10 mm long and 0.5 mm wide, fabricated with the optimum structure [Py (100 nm)/Ti (6 nm)]4/Cu (400 nm)/[Ti (6 nm)/Py (100 nm)]$_4$.

In any case, in most situations it is not necessary to exactly match the material parameters to obtain very useful information from FEM simulations. In the work described in Ref. [53], FEM was used to determine the optimum configuration of layers to maximize the MI response. The value of μ_{max} used in the simulations (μ_{max} = 5000 μ_0) was chosen quite arbitrarily but the resulting layer configuration was afterward fabricated, producing record values for both MI ratio and sensitivity for thin film structures with open-flux configuration. If fact, the permeability value used in FEM was underestimated since the measured MI values were larger than those obtained in the simulations. **Figure 10** illustrates these results. It is remarkable that the shape of the measured and simulated curves is, at least qualitatively, identical in the whole frequency range. This could not have been possible without including the measuring circuit (represented by the microstrip elements) in the simulation.

5. Application of thin film MI sensors

5.1. Brief survey of applications

The extremely large sensitivity of the MI effect makes it a good candidate for magnetic sensing applications, comparing favorably with other types of devices as Hall, anisotropic magnetoresistance (AMR), and giant magnetorresistance (GMR) sensors, and competing with fluxgate sensors [69].

MI devices based on amorphous wires have been successfully commercialized by Aichi Corporation as magnetic field sensors for motion, attitude, and acceleration detection [70]. Despite the easier integration of thin film-based structures with microelectronic circuitry, no commercial applications of thin film MI sensors can be found yet. As a pure magnetic field sensor, the application of thin films as an electronic magnetic compass has been evaluated [71].

The MI effect has also been proposed for the detection of magnetic particles, mainly oriented toward possible biomedical applications. Those were exhaustively reviewed recently [72]. Among the different materials used, besides wires and ribbons, thin film structures have been demonstrated to be able to detect microparticles in a flowing liquid [73] and nanoparticles embedded in gels (ferrogel) [74]. In these works, the presence of magnetic particles modifies the magnetic permeability on the medium surrounding the MI element, producing the measured changes in the impedance. Note that there is no direct measurement of the fringe field created by the particles, since no external magnetic field is applied to magnetize them. The field used to bias the sensing element (H_B in **Figure 1**) is not enough for that end. In fact, the electrical impedance of nonmagnetic conductors also varies in the presence of magnetic particles and this effect has been proposed as an alternative method for biosensing [75]. More sensitivity is expected if the fringe field of the particles is measured directly using the MI effect as a magnetic field detector. There is no inconvenient, in principle, in using thin film sensors substituting magnetic wires in the set-up described in Ref. [76].

MI has also been proposed as sensing mechanism for nondestructive testing (NDT), using amorphous wires [77] and thin film structures [78, 79], and even for pressure sensors using thin films deposited on a flexible substrate [40]. In fact, the use of flexible substrates for thin

film MI implementations is gaining relevance with the onset of applications of flexible electronics [39–42]. Novel deformation sensors are being proposed based on stress-impedance effect, which is very close to the MI effect, but based on the variations of the magnetic permeability experienced by the sensing material upon the application of mechanical strains [80, 81].

5.2. Circuit conditioning: impedance matching

The ultimate goal of the application of the MI effect is to develop a device that can compete in some aspect (sensitivity, miniaturization, prize, etc.) with the family of magnetic sensors that are widely used nowadays. Obviously, the circuit architecture in an industrially produced MI sensor would differ from the set-up implemented in the laboratory experiments. One of the aspects that would be benefited from a different circuit approach in a commercial device is the fact that the load impedance of the sensing element should be matched to the characteristic impedance of the transmission line, typically 50 Ω. The main goal of this procedure is to minimize the power consumption of the electronics, but in the case of a MI sensor it produces the additional benefit of an increased sensitivity. Matching the circuit load to 50 Ω is achieved by introducing impedance-matching networks in the circuit, typically consisting of *L* and *C* elements whose values are calculated to drive the impedance of the sample at the operation point (in general, complex) to 50 Ω (purely resistive) [82]. Thus, the imaginary part of the impedance of the sample gets cancelled with the addition of the *LC* network. As explained in Section 3.2, the imaginary part of the impedance is much less sensitive than the real part, due to the contribution of the external inductance. Therefore, by cancelling it and operating effectively with a purely resistive device, the MI ratio and sensitivity of the sample get noticeably improved. An example of this procedure applied to MI thin films, together with detailed calculations and results, can be found in Ref. [83].

5.3. Magnetic noise in thin film MI sensors

The parameter that really allows a faithful performance comparison between different magnetic sensors is their level of magnetic noise, which determines the threshold for the minimum signal level that can be reliably detected. Noise levels below 1 pT/√Hz can be obtained in MI sensors based on amorphous wires and ribbons [84, 85], but very little work has been done on determining the noise level in thin film-based structures. In a real application, the MI element is inserted in a conditioning circuit that, in its simplest configuration, is composed of a RF oscillator (that produces the ac current exciting the MI sensitive element), a detector, and an amplifier [86]. Each of these elements contributes to the total noise of the device. In an attempt to determine the noise of a thin film structure (a sandwiched multilayer 2 mm long and 90 μm wide with a sensitivity of 55%/Oe), the magnetic noise has been measured using different detectors: a commercial AD8302 Gain and Phase detector, a commercial power detector ZX47-50+, and a homemade peak detector [87]. The impedance of the sample is matched to 50 Ω using a specific matching network, to increase its sensitivity, as explained in the previous section. The measured electrical noise e_n is transformed in magnetic noise b_n expressed in T/√Hz through the experimentally determined transfer function of the sensor, that is, the relation between the input (magnetic field) and the output (voltage signal) of the device. The sensor using the peak detector displayed the lowest noise level of 3 nT/√Hz at 1 Hz and 122 pT/√Hz at 2 kHz, as shown in **Figure 11**.

http://dx.doi.org/10.5772/intechopen.70084

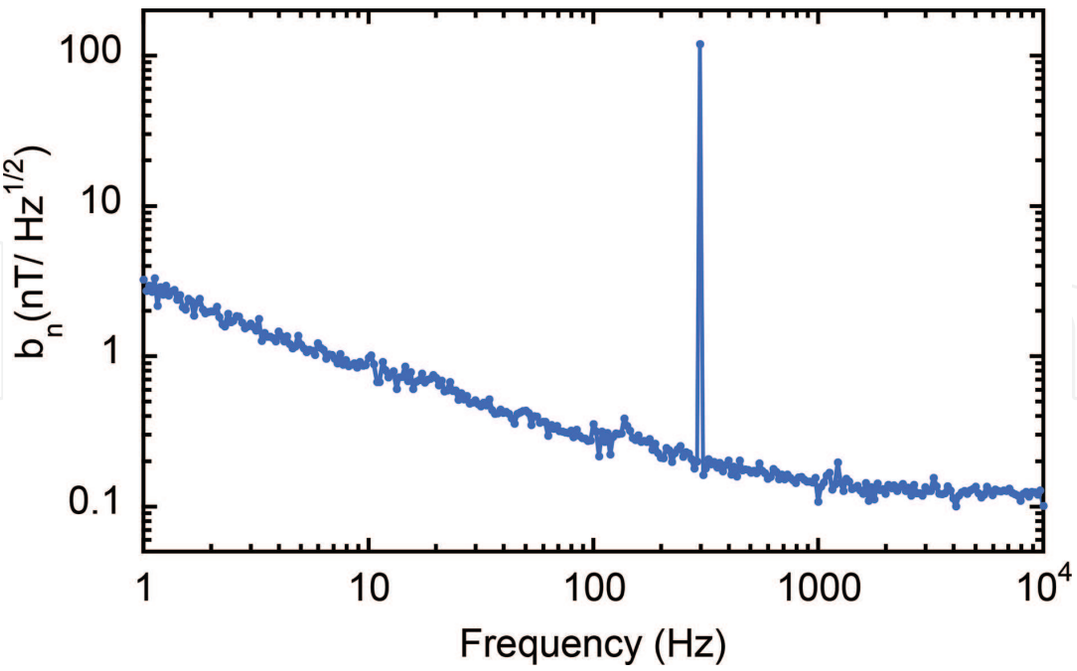


Figure 11. Equivalent magnetic noise measured in a thin film sandwiched multilayer sample, 2 mm long and 90 μm wide with structure [Py (170 nm)/Ti (6 nm)]$_3$/Cu (250 nm)/[Ti (6 nm)(Py (170 nm)]$_3$.

These noise levels are significantly larger than the ones reported in wires and ribbons [84, 85], but are promising for applications. Besides, the noise level can be reduced easily by a factor of 4 by using MI thin films with enhanced sensitivities (up to 300%/Oe), as the ones described recently [53]. Additionally, lower total noise values are expected by minimizing the RF oscillator contribution to noise [88].

6. Conclusions

Thin film structures displaying the magneto-impedance effect are already mature for sensing applications. Once their performance has reached levels comparable to those of amorphous wires, their fabrication compatibility with the microelectronic production processes makes them attractive for integrated devices. We have briefly reviewed the main concepts involved in the development of MI materials for future sensors. Many more details can be found in the proposed references, especially in the thesis reports by David de Cos [56] and Eduardo Fernández [88], on which much of the presented work is based.

Acknowledgements

Parts of the work summarized here have been performed thanks to the financial support from the Basque Government under grants KK-2016/00097 (Actimat Project) and KK-2016/00030 (Micro4Fab Project).

Author details

Alfredo García-Arribas[1,2]*, Eduardo Fernández[2,3] and David de Cos[4]

*Address all correspondence to: alfredo.garcia@ehu.es

1 Department of Electricity and Electronics, University of the Basque Country UPV/EHU, Leioa, Spain

2 Basque Centre for Materials, Applications and Nanostructures BCMaterials, Bizkaia Science and Technology Park, Derio, Spain

3 Department of Materials Science and Engineering, Massachusetts Institute of Technology, Cambridge, USA

4 Department of Applied Physics II, Faculty of Pharmacy, University of the Basque Country UPV/EHU, Vitoria, Spain

References

[1] Beach RS, Berkowitz AE. Giant magnetic field dependent impedance of amorphous FeCoSiB wire. Applied Physics Letters. 1994;**64:**3652

[2] Panina LV, Mohri K. Magneto-impedance effect in amorphous wires. Journal of Applied Physics. 1994;**65**:1189

[3] Lord Rayleigh. On the behaviour of iron and steel under the operation of feeble magnetic forces. Philosophical Magazine. 1887;**23**:225

[4] Kittel C. Theory of the dispersion of magnetic permeability in ferromagnetic materials at microwave. Physical Review. 1946;**70**:281

[5] Sommerfeld A. Electrodynamics. New York: Academic; 1952. p. 166

[6] Landau LD, Lifshitz EM. Electrodynamics of Continuous Media. Oxford: Pergamon; 1975. p. 211

[7] Chen D-X, Muñoz JL. AC impedance and circular permeability of slab and cylinder. IEEE Transactions on Magnetics. 1999;**35**:1906

[8] Cullity BD. Introduction to Magnetic Materials. 2nd ed. Menlo Park, California: Wiley-IEEE Press; 2009. p. 226

[9] Vázquez M. Soft magnetic wires. Physica B. 2001;**299**:302

[10] Vázquez M. Giant magneto-impedance in soft magnetic "wires". Journal of Magnetism and Magnetic Materials. 2001;**226-230**:693

[11] Vázquez M, Hernando A. A soft magnetic wire for sensor applications. Journal of Physics D: Applied Physics. 1996;**29**:939

[12] Machado FLA, Rezende SM. A theoretical model for the giant magnetoimpedance in ribbons of amorphous soft-ferromagnetic alloys. Journal of Applied Physics. 1996;**79**:6558

[13] Hernando B, Sánchez ML, Prida VM, Tejedor M, Vázquez M. Magnetoimpedance effect in amorphous and nanocrystalline ribbons. Journal of Applied Physics. 2001;**90**:4783

[14] Hika K, Panina LV, Mohri K. Magneto-impedance in sandwich film for magnetic sensor heads. IEEE Transactions on Magnetics. 1996;**32**:4594

[15] Morikawa T, Nishibe Y, Yamadera H, Nonomura Y, Takeuchi M, Taga Y. Giant magneto-impedance effect in layered thin films. IEEE Transactions on Magnetics. 1997;**33**:4367

[16] Antonov A, Gadetsky S, Granovsky A, D'yatckpv A, Sedova M, Perov N, Usov N, Furmanova T, Lagar'kov A. High-frequency giant magneto-impedance in multilayered magnetic films. Physica A. 1997;**241**:414

[17] Kurlyandskaya GV, Yakabchuck H, Kisker E, Bebenin NG, García-Miquel H, Vázquez M, Vas'kovskiy VO. Very large magnetoimpedance effect in FeCoNi ferromagnetic tubes with high order magnetic anisotropy. Journal of Applied Physics. 2001;**90**:6280

[18] Gromov A, Korenivski V. Electromagnetic analysis of layered magnetic/conductor structures. Journal of Physics D: Applied Physics. 2000;**33**:773

[19] Panina LV, Makhnovskiy DP, Maps DJ, Zarechnyuk DS. Two-dimensional analysis of magnetoimpedance in magnetic/metallic multilayers. Journal of Applied Physics. 2001; **89**:7221

[20] Fernández E, García-Arribas A, Volchkov SO, Kurlyandskaya GV, Barandiaran JM. Differences in the magneto-impedance of FeNi/Cu/FeNi multilayers with open and closed magnetic path. IEEE Transactions on Magnetics. 2010;**46**:658

[21] Morikawa T, Nishibe Y, Yamadera H, Nonomura Y, Takeuchi M. Sakata J, Taga Y. Enhancement of giant magneto-impedance in layered film by insulator separation. IEEE Transactions on Magnetics. 1996;**32**:4965

[22] Yu J, Zhou Y, Cai B, Xu D. Giant magneto-impedance effect in amorphous magnetostrictive FeSiB thin films. Journal of Magnetism and Magnetic Materials. 2000;**213**:32

[23] Nishibe Y, Yamadera H, Ohta N, Tsukada K, Ohmura Y. Magneto-impedance effect of a layered CoNbZr amorphous film formed on a polyimide substrate. IEEE Transactions on Magnetics. 2003;**39**:571

[24] Correa MA, Bohn F, Viegas ADC, Carara MA, Schelp LF, Sommer RL. Giant magneto-impedance in FM/SiO_2/Cu/SiO_2/FM films at GHz frequencies. Journal of Magnetism and Magnetic Materials. 2008;**320**:e25

[25] Tumanski S. Thin Film Magnetoresistive Sensors. London: IoP publishing; 2001

[26] Sugita Y, Fujiwara H, Sato T. Critical thickness and perpendicular anisotropy of evaporated films with stripe domains. Applied Physics Letters. 1967;**10**:229

[27] Coïsson M, Vinal F, Tiberto P, Celegato F. Magnetic properties of FeSiB thin films displaying stripe domains. Journal of Magnetism and Magnetic Materials. 2009;**321**:806

[28] Svalov AV, Aseguinolaza IR, García-Arribas A, Orue I, Barandiaran JM, Alonso J, Fernández-Gubieda ML, Kurlyandskaya GV. Structure and magnetic properties of thin film Permalloy films near the "transcritical" state. IEEE Transactions on Magnetics. 2010;**46**:333

[29] Corrêa MA, Viegas ADC, da Silva RB, de Andrade AMH, Sommer RL. Magnetoimpedance of single and multilayered FeCuNbSiB films in frequencies up to 1.8 GHz. Journal of Applied Physics. 2007;**101**:043905

[30] Kurlyandskaya GV, Svalov AV, Fernández E, García-Arribas A, Barandiaran JM. Journal of Applied Physics. 2010;**107**:09C502

[31] Svalov AV, Fernández E, García-Arribas A, Alonso J, Fdez-Gubieda ML, Kurlyandskaya GV. Applied Physics Letters. 2012;**100**:162410

[32] Kurlyandskaya GV, García-Arribas A, Fernández E, Svalov AV. Nanostructured magnetoimpedance multilayers. IEEE Transactions on Magnetics. 2012;**48**:1375

[33] Ohmori K, Tan K, Itoi K, Nagasu K, Uemichi Y, Aizawa T, Yamauchi R. Thin film magneto-impedance sesnor integrated into $L1_0$ FePt thin film bias magnet. IEEE Transactions on Magnetics. 2008;**44**:3977

[34] García C, Florez JM, Vargas P, Ross CA. Asymmetrical giant magnetoimpedance in exchange-biased NiFe. Applied Physics Letters. 2010;**96**:232501

[35] Svalov A, Savin P, Lepalovskij V, Larrañaga A, Vas'kovskiy V, García-Arribas A, Kurlyandskaya G. Tailoring the exchange bias in FeNi/FeMn bilayers by heat treatment and FeMn surface oxidation. IEEE Transactions on Magnetics. 2014;**50**:2003904

[36] Corrêa MA, Bohn F, da Silva RB, Sommer RL. Magnetoimpedance effect at the high frequency range for the thin film geometry: Numerical calculation and experiment. Journal of Applied Physics. 2014;**116**:243904

[37] Wang T, Lei C, Lei J, Yang Z, Zhou Y. Preparation of meander thin-film microsensor and investigation of structural parameters on the giant magnetoimpedance effect. Applied Physics A. 2012;**109**:205

[38] Takayama A, Umehara T, Yuguchi A, Kato H, Mohri K, Uchiyama T. Integrated thin film magneto-impedance sensor head using plating process. IEEE Transactions on Magnetics. 1999;**35**:3643

[39] Kurlyandskaya GV, Fernández E, Svalov A, Burgoa Beitia A, García-Arribas A, Larrañaga A. Flexible thin film magnetoimpedance sensors. Journal of Magnetism and Magnetic Materials. 2016;**415**:91

[40] Fernández E, Kurlyandskaya GV, García-Arribas A, Svalov AV. Nanostructured giant magneto-impedance multilayers deposited onto flexible substrates for low pressure sensing. Nanoscale Research Letters. 2012;**7**:230

[41] Agra K, Mori TJA, Dorneles LS, Escobar VM, Silva UC, Chesman C, Bohn F, Corrêa MA. Dynamic magnetic behavior in non-magnetostrictive multilayered films grown on glass and flexible substrates. Journal of Magnetism and Magnetic Materials. 2014;**355**:136

[42] Li B, Kavaldzhiev MN, Kosel J. Flexible magnetoimpedance sensor. Journal of Magnetism and Magnetic Materials. 2015;**378**:499

[43] García-Arribas A, Fernández E, Barrainkua A, Svalov AV, Kurlyandskaya GV, Barandiaran JM. Comparison of micro-fabrication routes for magneto-impedance elements: Lift-off and wet-etching. IEEE Transactions on Magnetics. 2012;**48**:1601

[44] Giouroudi I, Hauser H, Musiejovsky L, Steurer J. Development of amorphous thin film meander trilayers and investigation of GMI effect. Proceedings of IEEE Sensors 2004. 2004;**2**:1024

[45] Kikuchi H, Oe S, Uetake H, Yabukami S, Nakai T, Hashi S, Ishiyama K. Enhancement of sensitivity on miniaturized thin-film magnetoimpedance with ellipsoidal element. Physics Procedia. 2015;**75**:1271

[46] Fernández E, López A, García-Arribas A, Svalov AV, Kurlyandskaya GV, Barrainkua A. High-frequency magnetoimpedance response of thin-film microstructures using coplanar waveguides. IEEE Transactions on Magnetics. 2015;**51**:1

[47] Fernández E, Svalov AV, Kurlyandskaya GV, García-Arribas A. GMI in nanostructured FeNi/Ti multilayers with different thicknesses of the magnetic layers. IEEE Transactions on Magnetics. 2013;**49**:18

[48] Volchkov SO, Fernández E, García-Arribas A, Barandiaran JM, Lepalovskij VN, Kurlyandskaya GV. Magnetic properties and giant magnetoimpedance of FeNi-based nanostructured multilayers with variable thickness of the central Cu lead. IEEE Transactions on Magnetics. 2011;**47**:3328

[49] García-Arribas A, Fernández E, Svalov AV, Kurlyandskaya GV, Barrainkua A, Navas D, Barandiaran JM. Tailoring the magnetic anisotropy of thin film permalloy microstrips by combined shape and induced anisotopropies. European Physical Journal B. 2013;**86**:136

[50] Kikuchi H, Kamata S, Nakai T, Hashi S, Ishiyama K. Influence of demagnetizing field on thin-film GMI magnetic sensor elements with uniaxial magnetic anisotropy. Sensors and Actuators B. 2015;**230**:142

[51] Makhnovskiy DP, Panina LV. Size effect on magneto-impedance in layered films. Sensors and Actuators A. 2000;**81**:91

[52] García-Arribas A, Fernández E, Orue I, Barandiaran JM. Determination of the distribution of transverse magnetic anisotropy in thin films from the second harmonic of Kerr signal. Applied Physics Letters. 2013;**103**:142411

[53] García-Arribas A, Fernández E, Svalov A, Kurlyandskaya GV, Barandiaran JM. Thin-film magneto-impedance structures with very large sensitivity. Journal of Magnetism and Magnetic Materials. 2016;**400**:321

[54] de Cos D, García-Arribas A, Barandiaran JM. Analysis of magnetoimpednace measurements at high frequency using a microstrip transmission line. Sensors and Actuators A. 2004;**115**:368

[55] de Cos D, Fry N, Orue I, Panina LV, García-Arribas A, Barandiaran JM. Very large magnetoimpedance (MI) in FeNi/Au multilayer film systems. Sensors and Actuators A. 2006;**129**:256

[56] de Cos D. Magento-impedancia de muestras planas en alta frecuencia (in spanish) [thesis]. Leioa, Spain: Universidad del País Vasco, UPV/EHU; 2006

[57] García-Arribas A, de Cos D, Barandiaran JM. Determination of the intrinsic high-frequency magnetoimpedance spectra of multilayer systems. Journal of Applied Physics. 2006;**99**:08C507

[58] Makhnovskiy DP, Panina LV, Mapps DJ. Field-dependent surface impedance tensor in amorphous wires with two types of magnetic anisotropy: Helical and circumferential. Physical Review B. 2001;**63**:144424

[59] Kraus L. Theory of giant magneto-impedance in the planar conductor with uniaxial magnetic anisotropy. Journal of Magnetism and Magnetic Materials. 1999;**195**:764

[60] Barandiaran JM, García-Arribas A, Muñoz JL, Kurlyandskaya GV, Valenzuela R. Domain wall permeability limit for the giant magnetoimpedance effect. Journal of Applied Physics. 2002;**91**:7451

[61] Kraus L. The theoretical limits of giant magneto-impedance. Journal of Magnetism and Magnetic Materials. 1999;**196**:354

[62] Barandiarán JM, García-Arribas A, Muñoz JL, Kurlyandskaya GV. Influence of magnetization processes and device geometry on the GMI effect. IEEE Transactions on Magnetics. 2002;**38**:3051

[63] Nejad SN, Mansour R. A 3D finite-element analysis of giant magnetoimpedance thin-film magnetic sensors. IEEE Transactions on Magnetics. 2016;**52**:4000208

[64] Li B, Kosel J. Three dimensional simulation of giant magneto-impedance effect in thin film structures. Journal of Applied Physics. 2011;**109**:07E519

[65] Sinnecker JP, Pirota KR, Knobel M, Kraus L. AC magnetic transport on heterogeneous ferromagnetic wires and tubes. Journal of Magnetism and Magnetic Materials. 2002;**249**:16

[66] García-Arribas A, Barandiarán JM, de Cos D. Finite element method calculations of GMI in thin films and sandwiched structures: Size and edge effects. Journal of Magnetism and Magnetic Materials. 2008;**320**:e4

[67] Meeker DC. Finite Element Method Magnetics, Version 4.2 [Internet]. 12 January 2016 Build. Available from: http://www.femm.info

[68] Crozier R, Mueller M. A New MATLAB and Octave interface to a popular magnetics finite element code. Proceedings of the 22nd International Conference on Electric Machines (ICEM 2016); 4-7 Sept. 2016; Lausanne, Switzerland. IEEE; 2016

[69] Ripka P, Janosek M. Advances in magnetic field sensors. IEEE Sensors Journal. 2010; **10**:1108

[70] Mohri K, Uchiyama T, Panina L V, Yamamoto M, and Bushida K, Recent Advances of Amorphous Wire CMOS IC Magneto-Impedance Sensors: Innovative High-Performance Micromagnetic Sensor Chip. Journal of Sensors. 2015;**2015**:718069

[71] García-Arribas A, Fernández E, Orue I, de Cos D, Barandiaran JM, Michelena JM, Martínez F. Evaluation of a thin film giant magneto-impedance electronic compass. Sensor Letters. 2013;**11**:36

[72] Wang T, Zhou Y, Lei C, Luo J, Xie S, Pu H. Magnetic impedance biosensor: A review. Biosensors and Bioelectronics. 2017;**90**:418

[73] García-Arribas A, Martínez F, Fernández E, Ozaeta I, Kurlyandskaya GV, Svalov AV, Berganzo J, Barandiaran JM. GMI detection of magnetic-particle concentration in continuous flow. Sensors and Actuators A. 2011;**172**:103

[74] Kurlyandskaya GV, Fernández E, Safronov AP, Svalov AV, Beketov I, Burgoa Beitia A, García-Arribas A, Blyakhman FA. Giant magnetoimpedance biosensor for ferrogel detection: Model system to evaluate properties of natural tissue. Applied Physics Letters. 2015;**106**:193702

[75] Lago-Cachón D, Rivas M, Martínez-García JC, García JA. Cu impedance-based detection of superparamagnetic nanoparticles. Nanotechnology. 2013;**24**:245501

[76] Fodil K, Denoual M, Dolabdjian C, Treizebre A, Senez V. In-flow detection of ultra-small magnetic particles by an integrated giant magnetic impedance sensor. Applied Physics Letters. 2016;**108**:173701

[77] Vacher F, Alves F, Gilles-Pascaud C. Eddy current nondestructiuve testing with giant magneto-impedance sensor. NDT&E International. 2007;**40**:439

[78] Barandiaran JM, Kurlyandskaya GV, de Cos D, García-Arribas A, Vas'kovskiy VO. Multilayer magnetoimpedance sensor for nondestructive testing. Sensor Letters. 2009;**7**:374

[79] Moulin J, Dufourg-Gergam E, Oubensaid E-H, Alves F, Kaviraj B, Gupta A, Reddy VR, Barrué R. Realisation of micro-patterned multi-element magneto-impedance sensors for non destructive testing. Sensor Letters. 2009;**7**:272

[80] Agra K, Bohn F, Mori TJA, Callegari GL, Dorneles LS, Correa MA. Handling magnetic anisotropy and magnetoimpedance effect in flexible multilayers under external stress. Journal of Magnetism and Magnetic Materials. 2016;**420**:81

[81] García-Arribas A, Combarro L, Goiriena-Goikoetxea M, Kurlyandskaya GV, Svalov AV, Fernández E, Orue I, Feuchtwanger J. Thin-film magnetoimpedance structures onto flexible substrates as deformation sensors. IEEE Transactions on Magnetics. 2017;**53**:2000605

[82] Bowick C. RF Circuit Design. 1st ed. Indianapolis: Howards Sms & Co; 1982

[83] de Cos D, Sandacci SI, García-Arribas A, Barandiaran JM. Impedance matching networks for power transfer and sensitivity enhancement in GMI sensors. IEEE Transactions on Magnetics. 2005;**41**:3655

[84] Dufay B, Saez S, Dolabdjian CP, Yelon A, Menard D. Characterization of an optimized off-diagonal GMI-based magnetometer. IEEE Sensors Journal. 2013;**13**:379

[85] Malatek M, Dufay B, Saez S, Dolabdjian C. Improvement of the off-diagonal magneto-impedance sensor white noise. Sensors and Actuators A. 2013;**204**:20

[86] Ding L, Saez S, Dolabdjian C, Melo LGC, Yelon A, Ménard D. Equivalent magnetic noise limit of low-cost GMI magnetometer. IEEE Sensors Journal. 2009;**9**:159

[87] Fernández E, García-Arribas A, Barandiaran JM, Svalov AV, Kurlyandskaya GV, Dolabdjian CP. Equivalent magnetic noise of micro-patterned multilayer thin films based GMI microsensor. IEEE Sensors Journal. 2015;**15**:6707

[88] Fernández E. Thin-film magnetoimpedance micro-structures for sensing applications [thesis]. Leioa, Spain: Universidad del País Vasco, UPV/EHU; 2016

IntechOpen